Int. Journal of Refractory Metals and Hard Materials 45 (2014) 212–217

Contents lists available at ScienceDirect

Int. Journal of Refractory Metals and Hard Materials

journal homepage: www.elsevier.com/locate/IJRMHM

# Thermal dependence of elastic properties of polycrystalline $TiC_{0.97}$ and $TiC_{0.40}N_{0.60}$ alloys studied by surface Brillouin scattering

B.A. Mathe [a,b], J.D. Comins [b], A.G. Every [a], W. Lengauer [c,*]

[a] Materials Physics Research Institute, School of Physics, University of the Witwatersrand, Wits, Johannesburg 2050, South Africa
[b] DST/NRF Centre of Excellence in Strong Materials, University of the Witwatersrand, Wits, Johannesburg 2050, South Africa
[c] Institute for Chemical Technologies and Analytics, Vienna University of Technology, Vienna, Austria

ARTICLE INFO

*Article history:*
Received 17 December 2013
Accepted 12 April 2014
Available online 26 April 2014

*Keywords:*
Surface Brillouin scattering
Rayleigh surface acoustic wave
Acoustic phonons
Young's modulus
Bulk modulus
Poisson's ratio

ABSTRACT

Transition metal carbides, nitrides and carbonitrides form an interesting class of compounds having an exceptional combination of physical properties including high melting points, high hardness values, high electrical and thermal conductivities and metallic lustre. Experimental information on the temperature dependence of the elastic properties of titanium carbide and nitride is scanty, and on titanium carbonitrides practically it is non-existent. An investigation of the Young's modulus (E), shear modulus (G) and bulk modulus (B) of these non-textured, non-stoichiometric polycrystalline compounds ($TiC_{0.97}$ and $TiC_{0.40}N_{0.60}$) was conducted as a function of temperature, using surface Brillouin scattering (SBS). An approach utilising Rayleigh SAWs and an assumed Poisson's ratio was used to determine the elastic moduli E and B at room temperature as well as at high temperatures up to 700 °C. The variation of the elastic moduli with temperature points to the important influence of the intrinsic phonon–phonon interactions.



## Introduction

Refractory carbides, nitrides and carbonitrides of the Group IV transition metals are used as the hard phase in sintered cermet alloys and for protective layers on hard metals. It is well known that titanium carbides, nitrides and carbonitrides exhibit an exceptional combination of physical properties. Their electrical and thermal conductivities are close to those of pure metals. Their melting points allow one to consider them as refractory ceramics. Their chemical stability and corresponding hardness are among the highest, after that of diamond. In cermets, the mechanical characteristics of hard constituents critically influence the performance of the composites because they are subjected to loads not only at ambient conditions but also elevated temperatures [1,2]. The response to load and temperature cycling of the cermets is of importance and knowledge of Young's modulus, Poisson ratio, shear and bulk modulus is required in applications and engineering design. However, it is also important to recognise that there is very little experimental information on these carbonitrides [3–5] for one to make comparisons adequately. In addition, difficulties often encountered in carrying out adequate characterisation of specimens and systematic comparison of data include the preparation of nominally stoichiometric specimens and the control of their density [5]. In this paper, we have characterised the specimen using X-ray diffraction, measured the bulk density and compared with X-ray density to determine the degree of porosity of the specimen. Using surface Brillouin spectroscopy on the well-characterised titanium carbide and carbonitride samples, we have been able measure the change of elastic constants with temperature, and the results show that intrinsic phonon–phonon interactions contribute significantly to the total anharmonicity, for which we observe a stronger effect of these interactions in titanium carbide.

## Characterisation

The two samples, namely $TiC_x$ and $TiC_xN_y$ were each characterised as detailed below for the following parameters; carbon content/stoichiometry, density, porosity, and lattice structure. Both specimens were approximately $4 \times 4 \times 2$ mm$^3$ in size and were mechanically polished to a final surface finish of 0.25 μm and then ultrasonically cleaned. Bulk density of the specimen was measured using the Archimedes method. The values of the bulk density were obtained as $\rho = 4.836$ g/cm$^3$ for $TiC_{0.97}$ and $\rho = 4.730$ g/cm$^3$ for $TiC_{0.4}N_{0.6}$.

Investigations using a Philips PW1050 X-ray diffractometer system (Cu Kα) radiation (40 kV, 20 mA), conducted at room temperature, confirmed the NaCl/cubic crystal structure for both samples and yielded a lattice spacing of 4.330 Å and 4.270 Å for TiC and Ti(C,N) respectively as deduced from the spectra in Fig. 1(a) and (b). The present samples were prepared by hot-isostatic-pressing and no evidence of preferred orientation or texture was found by comparing the observed intensities

* Corresponding author at: Physical Metallurgy Group, Vienna University of Technology, Getreidemarkt 9/164CT, A-1060 Vienna, Austria. Tel.: +436641009019.
*E-mail address:* walter.lengauer@tuwien.ac.at (W. Lengauer).

http://dx.doi.org/10.1016/j.ijrmhm.2014.04.013
0263-4368/

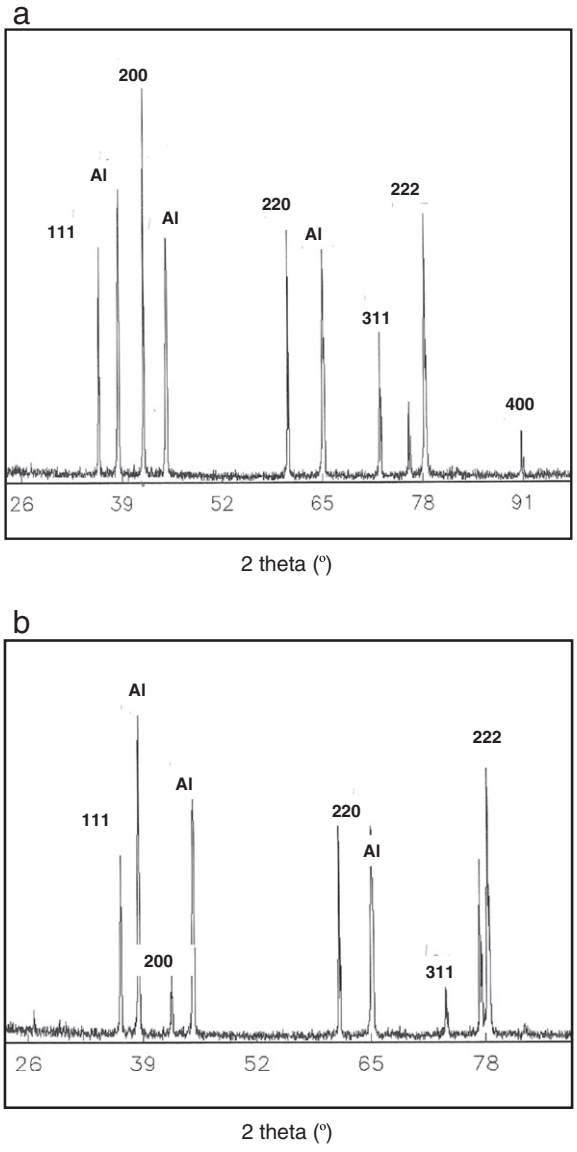


**Fig. 1.** (a): XRD spectrograph for the hot-pressed TiC sample taken using Cu radiation. The (200) peak was considered for the *d*-spacing calculations. Al reflections originate from the aluminium sample holder. (b): XRD spectrum for TiCN sample measured using Cu radiation (1.542 Å). The (200) peak was again considered for the *d*-spacing calculations. Al reflections observed also originate from the same aluminium sample holder.

from XRD scans with those of powder samples. This lattice spacing of Ti(C, N) compared very well with results reported in Ref. [5,6], of 4.251 Å for a related specimen with 7% porosity. The X-ray measured density was calculated to be 4.73 g/cm$^3$ from the unit cell volume, a value in excellent agreement with macroscopically determined value of 4.73 g/cm$^3$ (to within experimental error limits of the Archimedes method). The shift of the *d*-value of the {200} peak in the XRD spectra generally obeys Vegard's law in relation to the C / C + N concentration [6,7], and from these data the carbon concentration was estimated to be x ~ 0.4, giving the stoichiometry of the sample as $TiC_{0.4}N_{0.6}$. The almost zero porosity of the $TiC_{0.4}N_{0.6}$ was also indicative of the very low concentration of vacancies (<2%) existing in this sub-lattice as predicted by Rietveld refinement calculations applied to the non-metallic lattice of TiCN [4]. Similarly, analysis of the XRD results confirmed the f.c.c. NaCl-structure (B1) of the TiC specimen, having a lattice parameter of 4.330 Å from which a theoretical X-ray density of 4.899 g/cm$^3$ was obtained. This value of the density is quite close to the macroscopically determined value of bulk density of 4.836 g/cm$^3$, implying a better than 98.7% agreement in density for the specimen. Additionally, the density values reported above compare very well with the mean value stated in the CRC Handbook of Materials Science [8] for these compounds. The stoichiometry of the TiC sample was determined to be $TiC_{0.9}$ following the same approach of measuring the shift of the {200} peak. For all the calculations presented in the paper, the Archimedes values of the respective bulk densities of $TiC_{0.97}$ and $TiC_{0.4}N_{0.6}$ given above were used.

## SBS experimental

The majority of the surface Brillouin scattering measurements were carried out with the samples mounted within a specially designed high temperature optical vacuum furnace. A Spectra Physics 2060 argon ion laser was used to provide the p-polarised exciting light of wavelength $\lambda = 514.5$ nm. The samples were illuminated at an incident angle of 70.9°. The backscattered light was collected by a 120 mm focal length lens of aperture f/5.5 and focussed by the external optics of the Brillouin spectrometer into a Sandercock type (3 + 3) pass tandem Fabry–Pérot interferometer. A free spectral range of 30 GHz was used for all the measurements conducted in the optical furnace. A detailed description of the experimental arrangement may be found in Ref. [9].

These refractory materials proved challenging in terms of the measurement parameters owing to their high elastic light scattering and intense background noise in the recorded spectra. A careful balance was needed in the choice of the incident laser light intensity and the spectral accumulation time in the surface Brillouin scattering measurements. Even so, the background noise prevented the detection of additional modes besides the Rayleigh mode (see Figs. 2 and 3 below).

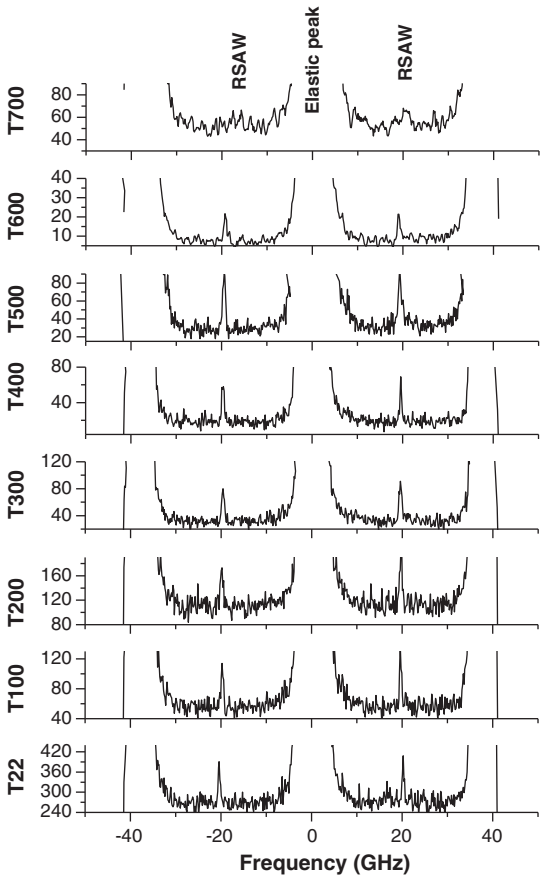


**Fig. 2.** Plot of temperature dependent SBS spectra for $TiC_{0.97}$ showing the Stokes and anti-Stokes Rayleigh SAW as the only experimentally observable mode. Note the ordinate scale which shows the decrease in peak intensity as temperature approaches 700 °C due to surface deterioration. Temperatures are indicated as follows: T100 = 100 °C etc.

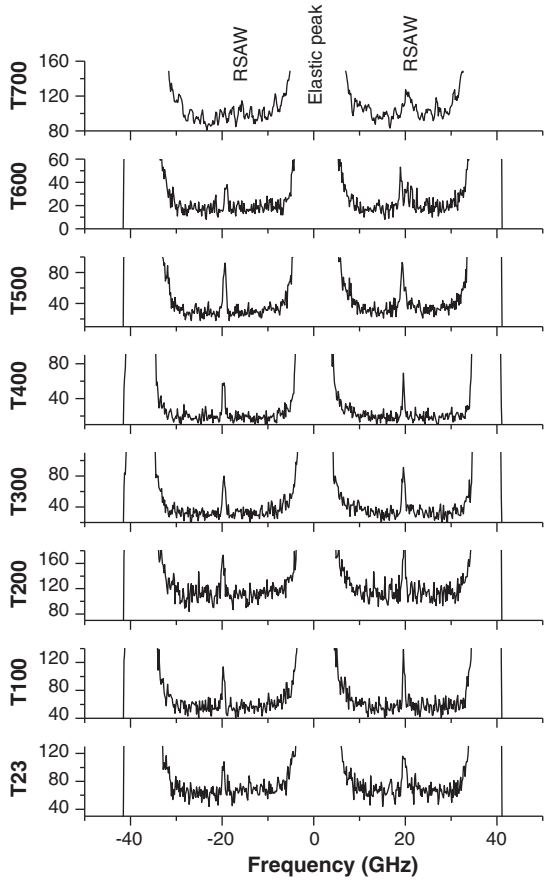


**Fig. 3.** Plot of temperature dependent SBS spectra for $TiC_{0.4}N_{0.6}$ showing the Stokes and anti-Stokes Rayleigh SAW as the only experimentally observable mode. Temperatures are indicated as follows: T100 = 100 °C etc.

In order to obtain the high temperature data, the sample was successively heated in the optical vacuum furnace at a series of temperatures ranging from room temperature to 700 °C and spectra collected at each chosen steady temperature (±1 °C) within a period of close to 30 min. The heating series was terminated after 700 °C, as the surfaces of the samples started to deteriorate due to oxidation effects leading to poor quality spectra.

## SBS theory and elasticity

Surface Brillouin scattering probes thermally excited acoustic phonons that are naturally present in the medium under investigation. In near opaque bulk samples and under favourable conditions, the major excitations observed by SBS are the Rayleigh surface acoustic wave (RSAW) and the Lamb shoulder being a continuum of excitations resulting from surface displacements induced by bulk modes [9,10]. However, as discussed above, SBS studies of polycrystalline Ti(C,N) and TiC, were restricted to the measurement of the Rayleigh SAW alone. Accordingly appropriate procedures were needed to determine their elastic properties.

In the backscattering geometry used, the incident angle $\theta_i$ is equal to the scattering angle $\theta_s$ (both denoted as $\theta$), and the velocity $V_R$ of the RSAW can be calculated from the equation:

$$\Delta f_R = \frac{2\sin\theta}{\lambda} V_R \tag{1}$$

where λ is the wavelength and $\Delta f_R$ is the measured Brillouin shift of the RSAW [9,10].

The acoustic wave velocity is related to the elastic constants by a generalised relation $X = \rho V^2$, where $X$ is a combination of elastic constants depending on the direction of propagation of the particular wave with respect to the crystallographic axes, and $\rho$ is the density. In the simplest case of an isotropic solid as appropriate for the present work, the matrix of the elastic constants is fully determined by two independent quantities; the only non-zero matrix elements are

$$C_{11} = C_{22} = C_{33},\ \ C_{44} = C_{55} = C_{66},\ \ C_{12} = C_{13} = C_{23} = C_{11} - 2C_{44}.$$

In this case the shear modulus G coincides with $C_{44}$, while Young modulus E, Poisson's ratio $\nu$ and bulk modulus B are respectively given by [9,11]

$$E = \frac{C_{44}(3C_{12} + 2C_{44})}{C_{12} + C_{44}} = \frac{C_{44}(3C_{11} - 4C_{44})}{C_{11} - C_{44}}$$
$$\upsilon = \frac{C_{12}}{C_{11} + C_{12}} = \frac{C_{11} - 2C_{44}}{2(C_{11} - C_{44})} = \frac{E}{2G} - 1$$

$$B = \frac{C_{11} + 2C_{12}}{3} = C_{11} - \frac{4}{3}C_{44}. \tag{2}$$

For elastic, isotropic media, the solution of the surface-wave equation is the implicit equation for the velocity of Rayleigh surface waves. To obtain expressions for the dependence of the Rayleigh velocity on the Poisson ratio or the material elastic constants, the procedure utilises the real roots of the Rayleigh wave equation solved as a function of the Poisson ratio. The procedure involves $V_R$, $V_T$ and $V_L$ being the Rayleigh, bulk transverse and bulk longitudinal velocities.

The exact dependence of the Rayleigh velocity ratio $V\left(=\frac{V_R}{V_T}\right)$ on the Poisson ratio $\upsilon$ and the bulk wave velocity ratio [11],

$$R = \frac{V_T}{V_L} = \sqrt{\frac{1-2\upsilon}{2(1-\upsilon)}} \tag{3a}$$

requires solving a cubic equation [11,12] derived from Eq. (3b) given below:

$$\left[\frac{2}{V^2} - 1\right]^2 = \frac{4}{V^2}\sqrt{\frac{1}{V^2} - 1}\sqrt{\frac{1}{V^2} - R^2}. \tag{3b}$$

A polynomial form of this equation can be written as a function of Poisson ratio thus;

$$V^6 - 8V^4 + 8V^2\left(\frac{2-\upsilon}{1-\upsilon}\right) - \frac{8}{(1-\upsilon)} = 0. \tag{4}$$

## Results and discussion

From Figs. 2 and 3, the Rayleigh mode is the only clearly observable mode with its frequency close to 20 GHz, and is identified by its linear relationship to sin $\theta$ as shown in Fig. 4 below. Also from Figs. 2 and 3 it is evident that the Rayleigh SAW (RSAW) decreases in frequency with increasing temperature. In theory, the intensity of the RSAW mode should increase with an increase in temperature due to the Bose–Einstein population factor. However, the gradual deterioration of surface quality due to oxidation in both samples results in reduced intensities, notwithstanding the technical challenges of maintaining the same focussing and positioning of the laser on the sample being heated in-situ. More importantly, the conclusions rely on frequency shifts, and these are accurately measured by the interferometric technique used.

Additionally, for each sample, measurements were also performed outside the furnace where several incident angles $\theta_i$ were used, usually

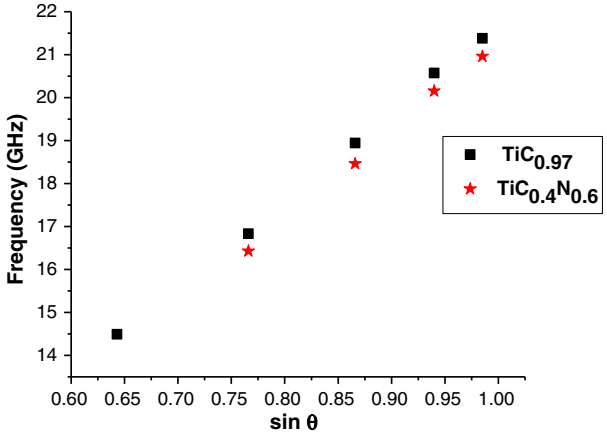


**Fig. 4.** Plot of the Rayleigh SAW frequency shift showing characteristic linear dependency on sin $\theta$, exhibited by scattering by surface acoustic waves (SAW).

from 20 to 80°, in order to investigate the dispersion of the surface acoustic modes (see Fig. 4). Since only one velocity, that of the Rayleigh SAW, was measured in the experiments, but there are two independent elastic parameters required to characterise the system, a value of the Poisson ratio has been assumed, allowing for the other elastic constant to be derived from the measured data. The value of Poisson's ratio of $TiC_{0.97}$ was selected as 0.170, independent of temperature, close to the value reported in the literature for sintered polycrystalline TiC [5,14]. This choice was informed by the near perfect stoichiometry, low concentration of vacancies and the high content of bonded carbon which is an indication of strength and hardness in refractory carbides [13,14]. Similar considerations based on the experimental results by Ivanov et al. [14], Lengauer [5], and the computational results of Ivaschenko et al. [7], as well as the almost zero porosity of the present sample, led to the choice of Poisson's ratio for the $TiC_{0.40}N_{0.60}$ specimen of 0.190, also independent of temperature. With these values of $\upsilon$ the Rayleigh equation (Eq. (4)) has an exact real solution for the velocity ratio, $V\left(=\frac{V_R}{V_T}\right) = 0.9058$ for the $TiC_{0.97}$ sample and $V = 0.9093$ for the $TiC_{0.40}N_{0.60}$ sample, yielding $V_t = 6260\ ms^{-1}$ and $6480\ ms^{-1}$ at room temperature for the two samples, respectively. From the corresponding values for $R$ obtained by solving Eq. (3a), the following values are obtained, namely $R(TiC_{0.97}) = 0.631$ and $R(TiC_{0.40}N_{0.60}) = 0.619$, for which values of longitudinal velocity ($V_L$) were determined at room temperature, as 9940 $ms^{-1}$ and 10,300 $ms^{-1}$ for the two samples, respectively. Considering the two samples as isotropic solids, only two elastic constants are required ($C_{11} = \rho V_L^2$, and $C_{44} = \rho V_t^2$) to compute the elastic moduli (E and B) using the relations in Eq. (2). Table 1 shows the full set of results of the computed elastic constants for $TiC_{0.97}$ and Table 2 provides similar data for $TiC_{0.40}N_{0.60}$.

It should be noted that the values of the transverse velocity and Young's modulus determined by the surface Brillouin scattering method do not depend very sensitively on the value of Poisson's ratio for the range $0.20 \leq \upsilon \geq 0.16$, as shown in Fig. 5(a) and (b) below, where a variation in the assumed Poisson's ratio by 18% changes the transverse velocity by less than 1% for the two materials.

For bulk materials or thin films of sufficient thickness, the true Rayleigh SAW peak has a Lorentzian line shape with a line-width of about 0.5 GHz. Peaks of this nature are shown in Figs. 2 and 3 for spectra measured from room temperature up to 700 °C. Fig. 5(a) and (b) shows the plot of the RSAW mode velocity measured at the different annealing temperatures. The respective spectra have been measured for the same data-accumulation times (~16 h). Within the same figures, in order to establish the dependence of the RSAW mode on Poisson's ratio for these samples, we also show the computed RSAW velocities at the indicated assumed values of Poisson's ratio. There is clearly an insignificant dependence.

The last spectrum acquired at each temperature is shown in Figs. 2 and 3, because it provides the stable RSAW peak for that set temperature and notably there is no significant change of the peak shape of the RSAW, while the phase velocity of the $TiC_{0.97}$ mode decreases by about 5% from room temperature to 500 °C. Beyond 600 °C, the Rayleigh SAW velocity decreases by up to 7% for $TiC_{0.97}$, while the mode velocity for $TiC_{0.4}N_{0.6}$ decreases by less than 2% during the same heating period. The reduced thermal response or reduced curvature in Fig. 5(b) of $TiC_{0.4}N_{0.6}$ is clearly attributable to the presence of nitrogen. Also, in the spectra shown in Figs. 2 and 3, the original sharp Rayleigh peak remains essentially unchanged in width up to 600 °C; hence we could not associate any obvious phase changes to these results. The observed softening of the mode velocity with temperature is a phenomenon normally associated with volume expansion as the material is

**Table 1**
Table below shows elastic data for $TiC_{0.97}$ ($\upsilon = 0.17$) computed at each temperature.

| Temp (°C) | $V_{Rayleigh}$ (m/s) | $V_{Transverse}$ (m/s) | $V_{Londitudinal}$ (m/s) | $C_{44}$ (GPa) | $C_{11}$ (GPa) | E (GPa) | B (GPa) |
|---|---|---|---|---|---|---|---|
| 23 | 5674 | 6264 | 9935 | 190 | 477 | 444 | 224 |
| 100 | 5455 | 6022 | 9552 | 175 | 441 | 410 | 207 |
| 200 | 5489 | 6060 | 9611 | 178 | 447 | 416 | 210 |
| 300 | 5442 | 6001 | 9519 | 175 | 439 | 409 | 206 |
| 400 | 5436 | 6008 | 9529 | 174 | 438 | 408 | 206 |
| 500 | 5386 | 5946 | 9431 | 171 | 430 | 400 | 202 |
| 600 | 5279 | 5828 | 9244 | 164 | 413 | 384 | 194 |
| 700 | 5020 | 5542 | 8790 | 149 | 374 | 348 | 176 |

**Table 2**
Table below shows elastic data for $TiC_{0.40}N_{0.60}$ ($\upsilon = 0.19$) computed at each temperature.

| Temp (°C) | $V_{Rayleigh}$ (m/s) | $V_{Transverse}$ (m/s) | $V_{longitudinal}$ (m/s) | $C_{11}$ (GPa) | $C_{44}$ (GPa) | B (GPa) | E (GPa) |
|---|---|---|---|---|---|---|---|
| 23 | 5890 | 6479 | 10,473 | 519 | 199 | 254 | 473 |
| 100 | 5890 | 6479 | 10,473 | 519 | 199 | 254 | 473 |
| 200 | 5920 | 6505 | 10,516 | 523 | 200 | 256 | 476 |
| 300 | 5870 | 6426 | 10,388 | 510 | 195 | 250 | 469 |
| 400 | 5840 | 6452 | 10,431 | 515 | 197 | 250 | 465 |
| 500 | 5780 | 6359 | 10,280 | 500 | 191 | 245 | 455 |
| 600 | 5780 | 6359 | 10,280 | 500 | 191 | 245 | 455 |
| 700 | 5700 | 6267 | 10,130 | 485 | 186 | 238 | 442 |

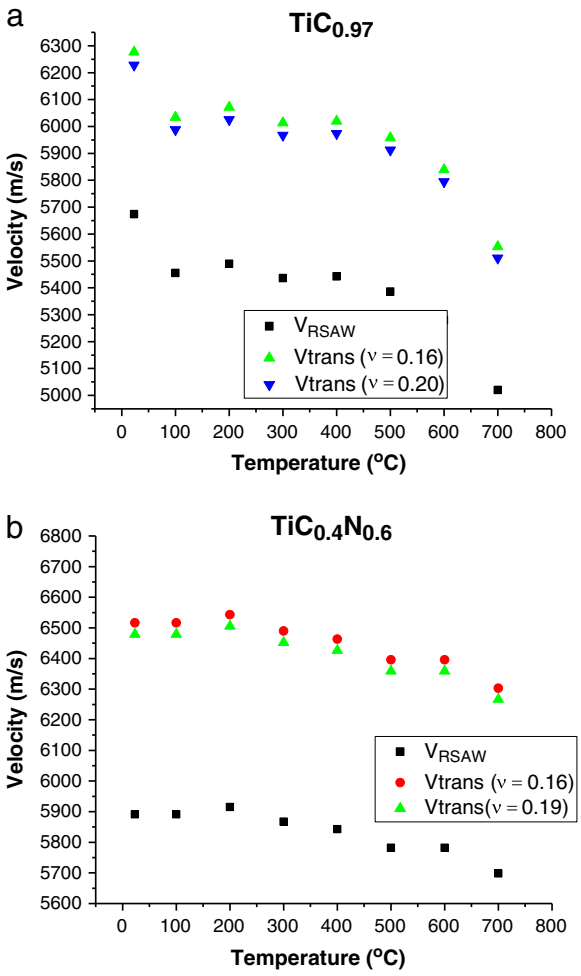


**Fig. 5.** (a): The variation of the measured RSAW velocity and computed transverse velocities is shown as a function of temperature for polycrystalline $TiC_{0.97}$. The fairly insignificant variation of the computed transverse velocities using different assumed Poisson's ratio values of 0.16 and 0.20 is shown. (b): The variation of the measured RSAW velocity and computed transverse velocities is shown as a function of temperature for polycrystalline $TiC_{0.40}N_{0.60}$. The fairly insignificant variation of the computed transverse velocities using different assumed Poisson's ratio values of 0.16 and 0.20 is shown.

heated up. In this respect the $TiC_{0.4}N_{0.6}$ sample shows a less rapid softening compared to $TiC_{0.97}$ and this response is directly correlated with the observed decrease in bulk moduli of this material.

Figs. 6 and 7 show the variation of the elastic moduli (E, G and B) with temperature for the two refractory materials. In all the computations, the density was regarded as a constant within the temperature range (298 K–1000 K) in light of the small temperature coefficient(s) of expansion (8.64 and 9.34) $\times 10^{-6}K^{-1}$ for $TiC_{0.9}$ and $TiC_{0.40}N_{0.60}$ respectively [15]. The room temperature elastic moduli values in Fig. 6 agree reasonably well with the results by Ivanov et al. [14], for the composition $TiC_{0.40}N_{0.60}$ which had a porosity of 3.3% and an ultrasonically determined Young's modulus of 459 GPa [5,14], taking cognisance of the differing porosity values. The results of the present investigation (E ~ 470 GPa) compare favourably with other reported results [5,14] while the additional strength in this sample can be attributed to the much smaller porosity.

For $TiC_{0.97}$, an approximately 20 GPa drop in the elastic moduli is observed in Fig. 7 when the sample is heated from ambient to 100 °C (over a measurement period of 16 h) which is thought to be associated with remnant sintering, comprised of remnants of un-dissolved TiC [16]. Thereafter the elastic moduli exhibit a quasi-monotonic decrease with temperature normally associated with phonon anharmonicity. Beyond

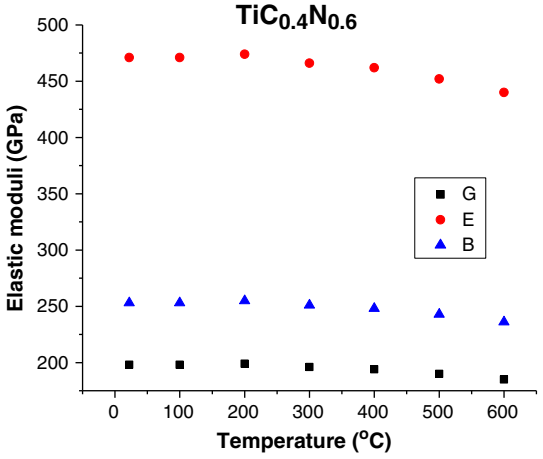


**Fig. 6.** The figure shows the variation of the Young's modulus (E), shear (G) and bulk moduli (B) of $TiC_{0.40}N_{0.60}$ with temperature showing a near linear decrease of the moduli, similar to results of Frantsevich et al. [17] on carbides.

about 500 °C for $TiC_{0.97}$, strong phonon–phonon coupling in the carbide is thought to contribute to the observed anomalous decrease in E and G. It is noted that similar behaviour has been observed for $NbC_{0.97}$ (with less than 5% porosity) and in tantalum carbide [5]. Generally, in non-stoichiometric refractory compounds the unscreened metal–metal bonds tend to appear due to the presence of vacancies in the metalloid sub-lattice, such as that of the titanium carbonitrides [7,14]. As the nitrogen concentration increases, there is a corresponding increase in the number of electrons available in metal–metal bonds, such that the unscreened metal–metal interactions can lead to a redistribution of vacancies in the metalloid sub-lattice leading to a significant increase in the short-range order of their arrangement. Such short range order which also locks the thermal distortions resulting in reduced sensitivity to thermal effects, can be associated with an increase in atomic interactions and hence an increase in bulk moduli. Ab initio elastic property calculations by Jhi and Ihm [13] predicted an increase of the bulk modulus as the nitrogen content increases for Ti(C,N) alloys. The present results affirm this prediction when the bulk moduli of the two alloys $TiC_{0.97}$ ($B = 220$ GPa) and $TiC_{0.40}N_{0.60}$ ($B = 254$ GPa) are compared together with Ivanov's results [14] where they reported

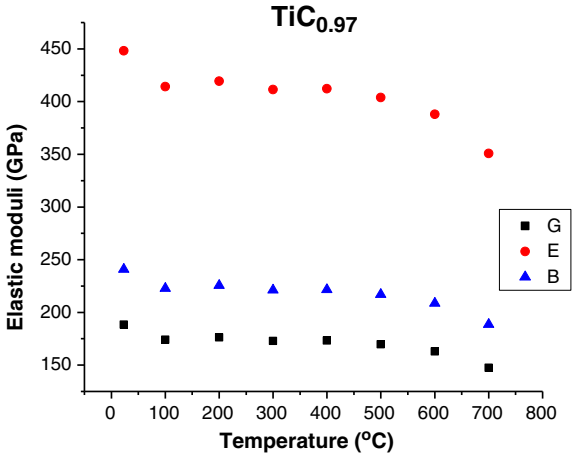


**Fig. 7.** The figure shows the variation of the Young's modulus (E), shear (G) and bulk moduli (B) for $TiC_{0.97}$ with temperature. An initial decrease is followed by the characteristic slower linear decrease associated with thermal expansion to about 500 °C. Subsequently an anomalous steep decrease associated with phonon anharmonicity is observed.

values consistently below 250 GPa for both $TiC_{0.97}$, and ($TiC_{0.4}N_{0.6}$ with a Poisson ratio of 0.19). (Owing to the significant reduction in the elastic constants between 20° and 100 °C in $TiC_{0.97}$ as discussed above, the comparison is made using the temperature of 100 °C in the present case).

## Conclusions

The room temperature elastic constants for $TiC_{0.40}N_{0.60}$, namely $C_{11} = 520$ ($\pm 10$) GPa and $C_{44} = 200$ ($\pm 8$) GPa compare favourably with computed results by Jhi and Ihm [13,18] for $TiC_{0.75}N_{0.25}$ where they reported the following single crystal elastic constants: $C_{11} = 553$ GPa, $C_{44} = 189$ GPa and $C_{12} = 128$ GPa. It is worth noting that the present results for the room temperature elastic moduli (E ~ 470 GPa, B ~ 250 GPa) (cf Fig. 6) lie mid-way in the solid-solutions $TiC_{0.5}N_{0.5}$ < (E,B) < $TiC_{0.25}N_{0.75}$, where each of the two alloy compositions represent upper and lower extremes for the reported elastic moduli in Ref. [7], respectively; i.e. E ranges from 460 GPa to 420 GPa, while B varies from 270 to 240 GPa. The increased strength of the present polycrystalline titanium carbonitride sample is thus attributable to the very low measured porosity of the specimen (<1%).

The elastic moduli of $TiC_{0.97}$ and $TiC_{0.40}N_{0.60}$ do not exhibit a quasi-linear behaviour predicted by classical quasi-harmonic theory as the temperature increases, but have a significant curvature, especially for $TiC_{0.97}$. These observations point to the fact that the intrinsic phonon–phonon interactions contribute to the total anharmonicity, an aspect that is normally neglected by the classical quasi-harmonic approximation used in models. These effects become prominent even at moderate temperatures near 400 °C for $TiC_{0.97}$.

## Acknowledgements

The authors wish to thank the DST/NRF Centre of Excellence in Strong Materials and the National Research Foundation of South Africa with Grant Number 2053306 for the financial support.

## References

[1] Toth LE. Transition metal carbides and nitrides. New York: Academic Press; 1971.
[2] Storms EK. The refractory carbides. New York: Academic Press; 1967.
[3] Lengauer W. Handbook of ceramic hard materials. In: Riedel R, editor. vol. 1. Weinheim: Wiley-VCH; 2000. p. 202–52.
[4] Levi G, Kaplan WD, Bamberger M. Structure refinement of titanium carbonitride. Mater Lett 1998;35:344–50.
[5] Kral C, Lengauer W, Rajafa D, Ettmayer P. Critical review on the elastic properties of transition metal carbides, nitrides and carbonitrides. J Alloys Compd 1998;265:215–33.
[6] Yang Q, Lengauer W, Koch T, Scheerer M, Smid I. Hardness and elastic properties of $Ti(C_xN_{1-x})$, $Zr(C_xN_{1-x})$ and $Hf(C_xN_{1-x})$. J Alloys Compd 2000;309:L5–9.
[7] Ivanschenko VI, Turchi PEA, Gonis A, Ivaschenko LA, Skrynskii PL. Electronic origin of elastic properties of titanium carbonitride alloys. Metall Mater Trans A 2006;37A:3391.
[8] CRC. Handbook of materials science. In: Lynch Charles T, editor. Vol II (metals, composites and refractory materials). , CRC Press; 1974–1980.
[9] Comins JD. Surface Brillouin scattering. Chapter 15 , Handbook of elastic properties of solids, liquids, and gases. , In: Levy M, Bass H, Stern R, Every AG, Sachse W, editors. Dynamic methods for measuring the elastic properties of solidsNew York: Academic Press; 2001. p. 187–226.
[10] Beghi MC, Every AG, Prakapenka VB, Zinin PV. Ultrasonic and electromagnetic NDE for structure and material characterisation. In: Kundu T, editor. Boca Raton, Florida: CRC; 2012. p. 539–610 [Chapter 10].
[11] Every AG. The elastic properties of solids: static and dynamic principles. Chapter 1 , Handbook of elastic properties of solids, liquids, and gases. , In: Levy M, Bass H, Stern R, Every AG, Sachse W, editors. Dynamic methods for measuring the elastic properties of solidsNew York: Academic Press; 2001. p. 3–36.
[12] Farnell GW, Mason WP, Thurston RN, editors. Physical acoustics, vol. 6. New York: Academic Press; 1970. p. 109–66.
[13] Jhi S-H, Ihm J. Electronic structure and structural stability of $TiC_xN_{1-x}$ alloys. Phys Rev 1997;B56:13826.
[14] Ivanov NA, Alyamovskii SI, Mitrofanov BV, Andreeva P. Elastic properties of nonstoichiometric titanium carbonitrides. Neorg Mater USSR 1976;12(7):1209–11.
[15] Aigner K, Lengauer W, Rafaja D, Ettmayer P. Lattice parameters and thermal expansion of $Ti(C_xN_{1-x})$, $Zr(C_xN_{1-x})$, $Hf(C_xN_{1-x})$ and $TiN_{1-x}$ from 298 to 1473 K as investigated by high-temperature X-ray diffraction. J Alloys Compd 1994;215:121–6.
[16] Upadhyaya GS. Nature and properties of refractory carbides. New York: Nova Science Publishers; 1996.
[17] Frantsevich IN, Zhurakovskii EA, Lyashchenko AB. Young's moduli of the carbides of some transition metals. Inorg Mater 1967;3:6.
[18] Krenn CR, Morris JW. Relationships between atomistic and intrinsic macroscopic hardness. In: Kumar A, Chung Y-W, Chia RWJ, editors. Hard coatings based on borides, carbides and nitrides; 1998. p. 379–88 [TMS].